

Inelastic energy loss of H_2^+ and H_3^+ ions correlated with molecular orientation

Toshiaki Kaneko

Department of Applied Physics, Okayama University of Science, 1-1 Ridaicho, Okayama 700, Japan

(Received 4 January 1994; revised manuscript received 19 August 1994)

Electronic stopping power of aluminum, carbon, and krypton were calculated for energetic H_2^+ and H_3^+ ions together with a diproton ($2H^+$) and a triproton ($3H^+$) with specific energies ranging from 1 keV/amu to 10 MeV/amu in a frozen charge state, based on the degenerate electron-gas model and the wave-packet model. It was found that for H_2^+ and $2H^+$ ions a strong orientation effect can be theoretically predicted on the stopping power S and the effective charge Z_{eff} . It was also clarified that the bound electrons significantly diminish the values of S and Z_{eff} , and that the velocity dependence of Z_{eff} is considerably weaker than that expected from the existing data. The values of S and Z_{eff} calculated for ~ 10 MeV/amu H_2^+ ion incident on carbon foils are found to be in good agreement with the recent experimental data.

PACS number(s): 34.50.Bw, 61.80.Mk

I. INTRODUCTION

The interaction of molecular ions with solids has been investigated intensively, in particular since about 20 years ago. The nonequilibrium charged fraction of the transmitted molecular ions gives information on the electron-capture and -loss cross sections and the survival probabilities [1–3]. At the same time, the molecular effects have been expected on various electronic excitations [4–7]. Regarding the inelastic energy loss, Brandt, Ratkowski, and Ritchie [8] first reported that the spatially correlated projectiles displayed considerably different aspects from the single-ion incidence. In the limit of the internuclear distance R being vanishing, the ion cluster acts as a unified single ion. On the other hand, in the limit of R being infinite, individual constituent ions in the cluster behave independently. Therefore, the values of R during the passage of the impinging cluster play an important role in the inelastic energy loss. So far, interest has been focused on the breakup of the cluster due to Coulomb explosion, following the electron stripping on entrance. In such a dissociation process, the spatial correlation of constituent particles varies as a function of the dwell time in a foil. Using the light-ion clusters, information on the initial internuclear separation and the internuclear force have been derived from the “ring pattern” [9–12] formed in the E - θ plane, where E and θ denote, respectively, the kinetic energy and the angle of the deflection of emerging particles. It was also reported [13] that the weak potential makes narrower the angular distribution of protons dissociated from the (${}^4\text{HeH}$) $^+$ ion than that expected only from the repulsive potential. In the research, an immediate stripping of the projectile electron(s) is a basic assumption. From the theoretical point of view, analyses based on the electron-gas model have been made to estimate the correlated energy loss of the cluster composed of bare point charges [8,14–16]. In these studies, the correlation is described by the interference (or the vicinage) function, which reveals that the energy loss per nucleon of the H_2^+ (H_3^+) ion relative to

that of a proton with the same velocity starts from 1.5 (2.0) and decreases monotonically to unity with increasing dwell time [8].

On the other hand, apart from dissociated charged particles, the transmission of the H_2^+ ions [17] and of the H_3^+ ions [18] has been reported. By interpreting the measured charge-fraction data, Cue *et al.* [17] concluded that there are two mechanisms incorporating in the 0.4–1.2 MeV/amu H_2^+ transmission. One is the original transmission without dissociation in superthin foils, and the other is the recombined process after dissociation occurred in thicker foils. Namely, in contrast to a rapid decrease of $\exp(-t_D/\tau)$ (t_D , dwell time; $\tau=0.17$ fs) of the former, the reduction of the latter is velocity dependent and more slow with the increasing of the foil thickness. Eckardt *et al.* [19] first observed that the energy loss per nucleon of 12.5–130 keV/u H_2^+ on carbon and aluminum is less than that of H^+ with the same specific energy. They concluded that it is due to the interference effects in the electron excitation by spatially correlated diprotons, whose internuclear distance is aligned close to the direction of motion. Levi-Setti, Lam, and Fox [20] reported that the stopping power for H_2^+ ions with velocities $v=0.7v_0$ (12.5 keV/amu) and $v=v_0$ (25 keV/amu) in carbon foils (0.3–1.1 $\mu\text{g}/\text{cm}^2$) relative to that for H^+ with the same velocity is greater than unity for the dissociation process while being less than unity for the recombination process. Here $v_0=2.19\times 10^8$ cm/s is the Bohr velocity. Using the MeV/atom energy O_2^+ and N_2^+ ions incident on carbon, Steuer *et al.* [21] also reported that the stopping power per atom is less than unity. This can be qualitatively explained [22] by assuming the internuclear distance R to be fixed at ~ 2 – $4 a_0$ ($a_0=0.529 \text{ \AA}$) in the electron-gas target. However, in order to get quantitatively good agreement with data, there is some room for further trials.

Recently, with the use of a high-resolution spectrometer, it became possible to directly measure the energy losses of the partially stripped charged particles, i.e., He^+ , $\text{C}^{4,5+}$, O^{5-7+} , with the same charge as the incident

[23–25]. In addition, the analytical formula derived on the basis of the first-order perturbation treatment is found to agree with the experimental data [26]. The energy loss of metastable ions with two electrons in the $1s2s$ configuration has also been investigated [27]. Under such circumstances, the information on the inelastic energy loss of the *originally transmitted* molecular ions is strongly expected to bring us a determination of to what extent the bound electron(s) diminish the inelastic energy-loss rate in comparison with bare clusters. Especially in super-thin foils, the energy loss of originally transmitted hydrogen molecules will interest us from the viewpoint of getting new knowledge.

In this paper, we report the energy loss of the originally transmitted H_2^+ and H_3^+ ions with the bound electron(s) being attached in solids and in a gas. The bound electron is described in a quantum-mechanical molecular-orbital treatment. These results are compared with the energy losses of diprotons and triprotons under the same internuclear distances. Hereby, the effective screening charge per projectile electron is also estimated. In Sec. II, our calculation method is developed with the determination of the bound-electron distribution. Section III is devoted to a presentation of results and a comparison with the recent experimental data. A discussion is also given there. Hereafter, we adopt atomic units ($e = m = \hbar = 1$) unless otherwise stated.

II. ENERGY-LOSS CALCULATION

A. Electron distribution of molecular ions

Let us start with the description of the bound electron on a H_2^+ ion. The wave function for a ground-state molecular orbital $1s\sigma_g$ is assumed to be

$$\begin{aligned}\psi_2(\mathbf{r}) &= N_2[\varphi(\mathbf{r}_1) + \varphi(\mathbf{r}_2)] , \\ \varphi(\mathbf{r}) &= (2\alpha/\pi)^{3/4} \exp(-\alpha r^2) ,\end{aligned}\quad (2.1)$$

where $\mathbf{r}_1 = \mathbf{r} - \mathbf{R}/2$ and $\mathbf{r}_2 = \mathbf{r} + \mathbf{R}/2$ denote the position vectors of the bound electron measured from two constituent protons located at $\pm \mathbf{R}/2$. The normalization factor N_2 is given by $N_2 = [2\{1 + \exp(-\alpha R^2/2)\}]^{-1/2}$, where R is the internuclear separation. The orbital parameter α is determined together with R by a variational method. To do so, using Eq. (2.1), we calculated the total energy E_{tot} of our system, composed of the kinetic energy $E_{\text{kin}} = \langle \psi_2 | -(\frac{1}{2})\Delta | \psi_2 \rangle$, the potential energy $E_{\text{pot}} = \langle \psi_2 | -1/r_1 - 1/r_2 | \psi_2 \rangle$, and the nuclear repulsion en-

ergy $E_{\text{rep}} = 1/R$. In an explicit form, we have, using the variable $x = (2\alpha)^{1/2}R$,

$$E_{\text{tot}} = E_{\text{kin}} + E_{\text{pot}} + E_{\text{rep}} , \quad (2.2a)$$

$$E_{\text{kin}} = 3\alpha/2 - (\alpha x^2/4) \exp(-x^2/4) / \{1 + \exp(-x^2/4)\} , \quad (2.2b)$$

$$\begin{aligned}E_{\text{pot}} &= -(8\alpha/\pi)^{1/2} / \{1 + \exp(-x^2/4)\} \\ &\times \left[1 + (1/x) \int_0^x dt \exp(-t^2) \right. \\ &\quad \left. + (4/x) \exp(-x^2/4) \int_0^{x/2} dt \exp(-t^2) \right] ,\end{aligned}\quad (2.2c)$$

$$E_{\text{rep}} = (2\alpha)^{1/2} / x . \quad (2.2d)$$

Thus the total energy E_{tot} is obtained as a function of two parameters, α and R , i.e., $E_{\text{tot}} = E_{\text{tot}}(\alpha, R)$. Then via the procedure of numerically minimizing E_{tot} on the two-dimensional (α, R) plane, we have as a minimum $E_{\text{tot}} = -0.531$ a.u. at $\alpha = 0.430$ a.u. and $R = 2.05$ a.u. = 1.084 Å. This value is a bit greater than the result of $R = 1.06$ Å for the lowest vibrational state and lower than the vibrationally averaged distance $R = 1.29$ Å [8].

In a similar manner, for a ground-state H_3^+ ion, we can determine the orbital parameter α and the internuclear separation R . Here it is assumed that two bound electrons are in a ground state in a singlet molecular state with opposite spins. The spatial wave function for the electron is also described by the Gaussians as

$$\psi_3(\mathbf{r}) = N_3[\varphi(\mathbf{r}_1) + \varphi(\mathbf{r}_2) + \varphi(\mathbf{r}_3)] , \quad (2.3)$$

with the normalization factor $N_3 = [3\{1 + 2\exp(-\alpha R^2/2)\}]^{-1/2}$. Here three constituent protons are assumed to construct a rigorous triangular structure. The total energy of this system is composed of the kinetic energy $E_{\text{kin}} = \langle \psi_3 | -(\frac{1}{2})\Delta | \psi_3 \rangle$, the potential energy $E_{\text{pot}} = \langle \psi_3 | -1/r_1 - 1/r_2 - 1/r_3 | \psi_3 \rangle$, the nuclear repulsion energy $E_{\text{rep}} = 3/R$, and the electron-electron repulsion energy

$$E_{ee} = \langle \psi_3(\mathbf{r}_1)\psi_3(\mathbf{r}_2) | 1/r_{12} | \psi_3(\mathbf{r}_1)\psi_3(\mathbf{r}_2) \rangle .$$

Now, using a variable $x = (2\alpha)^{1/2}R$, we have

$$E_{\text{tot}} = 2E_{\text{kin}} + 2E_{\text{pot}} + E_{\text{rep}} + E_{ee} , \quad (2.4a)$$

$$E_{\text{kin}} = 3\alpha/2 - (\alpha x^2/2) \exp(-x^2/4) / \{1 + 2\exp(-x^2/4)\} , \quad (2.4b)$$

$$\begin{aligned}E_{\text{pot}} &= -(8\alpha/\pi)^{1/2} \{1 + 2\exp(-x^2/4)\} \left[1 + (2/x) \int_0^x dt \exp(-t^2) \right. \\ &\quad \left. + (8/x) \exp(-x^2/4) \int_0^{x/2} dt \exp(-t^2) \right. \\ &\quad \left. + 4/\{(3)^{1/2}x\} \exp(-x^2/4) \int_0^{\sqrt{3}x/2} dt \exp(-t^2) \right] ,\end{aligned}\quad (2.4c)$$

$$E_{\text{rep}} = 3(2\alpha)^{1/2}/x . \quad (2.4d)$$

$$E_{\text{ee}} = 8(\alpha)^{1/2}/(3\pi) \{ 1 + 2 \exp(-x^2/4) \}^2 [\{ (\alpha)^{1/2}/4 \} \{ 1 + 4 \exp(-x^2/2) \} \\ + 1 / \{ (2)^{1/2}x \} F(x) + \{ 4(2)^{1/2}/x \} \{ 1 + \exp(-x^2/4) \} \exp(-x^2/4) F(x/2) \\ + 4 / \{ (6)^{1/2}x \} \exp(-x^2/4) F((3)^{1/2}x/2)] , \quad (2.4e)$$

with

$$F(x) = \int_0^\infty dy [\exp\{-(y-x)^2\} \\ - \exp\{-(y+x)^2\}] \int_0^y dz \exp(-z^2) . \quad (2.4f)$$

Thus we also find E_{tot} to be a function of two variables α and R via the parameter x . The integral can be estimated numerically by Simpson's method. By minimizing E_{tot} in a two-dimensional (α, R) plane, we obtain as a minimum $E_{\text{tot}} = -1.099$ a.u. at $\alpha = 0.475$ a.u. and $R = 1.695$ a.u. $= 0.897 \text{ \AA}$. This value of R is only 2% smaller than the result of the *ab initio* calculation, i.e., $R = 0.91396 \text{ \AA}$, by Carney and Porter [28]. They also have got a triangular structure with high accuracy ($\theta = 60.0012^\circ$), consistent with the present assumption. Judging from these situations, our results on R and α are reasonable, though a simpler method is employed. With further calculation, the value of α , describing the size of the bound electrons on the projectile, becomes essential as well as the value of R .

B. Electronic stopping power and effective charge

The inelastic energy loss of energetic H_2^+ and H_3^+ ions is estimated in a shellwise manner. Generally speaking, it is contributed from the conduction electrons and the core electrons. The former contribution is formulated in the RPA (random-phase-approximation) formalism [29], and the latter in the wave-packet theory [30]. These contributions are summed over all electronic shells. According to this theoretical procedure, the velocity and the Z_2 (target atomic number) dependence of the proton-stopping power values has been shown to agree with the experimental data [30–32]. In both treatments, the external ion charge expressed in the Fourier space plays an essential role. The local bound-electron distribution is given by $|\psi_2(\mathbf{r})|^2$ so that the total external charge of H_2^+ ($Z_1 = 1$) in (\mathbf{r}, t) space is given by

$$\rho_{\text{ext}}(\mathbf{r}, t) = Z_1 \delta(\mathbf{r} - \mathbf{R}_0 - \mathbf{R}/2) \\ + Z_1 \delta(\mathbf{r} - \mathbf{R}_0 + \mathbf{R}/2) - |\psi_2(\mathbf{r})|^2 . \quad (2.5)$$

Then, the four-dimensional Fourier transform of it yields

$$\rho_{\text{ext}}(\mathbf{k}, \omega) = 2\pi \rho_{\text{ext}}(\mathbf{k}) \delta(\omega - \mathbf{k} \cdot \mathbf{v}) , \quad (2.6a)$$

$$\rho_{\text{ext}}(\mathbf{k}) = A(k) \cos(\mathbf{k} \cdot \mathbf{R}/2) - B(k) , \quad (2.6b)$$

$$A(k) = 2Z_1 - \exp(-k^2/8\alpha) / \{ 1 + \exp(-\alpha R^2/2) \} , \quad (2.6c)$$

$$B(k) = \exp(-k^2/8\alpha) \\ \times \exp(-\alpha R^2/2) / \{ 1 + \exp(-\alpha R^2/2) \} . \quad (2.6d)$$

Here $\mathbf{R}_0 = \mathbf{v}t$ denotes the position vector of the center of mass of a H_2^+ ion ($Z_1 = 1$). On the other hand, for a H_3^+ ion, one has

$$\rho_{\text{ext}}(\mathbf{r}, t) = Z_1 \delta(\mathbf{r} - \mathbf{R}_0 - \mathbf{a}) + Z_1 \delta(\mathbf{r} - \mathbf{R}_0 - \mathbf{b}) \\ + Z_1 \delta(\mathbf{r} - \mathbf{R}_0 - \mathbf{c}) - 2|\psi_3(\mathbf{r})|^2 . \quad (2.7)$$

The vectors \mathbf{a} , \mathbf{b} , and \mathbf{c} denote the position of three protons measured from the position \mathbf{R}_0 (the center of mass of H_3^+) and $|\mathbf{a}| = |\mathbf{b}| = |\mathbf{c}| = R/(3)^{1/2}$. Then the form factor of a H_3^+ intruder is

$$\rho_{\text{ext}}(\mathbf{k}) = C(k) \{ \exp(i\mathbf{k} \cdot \mathbf{a}) + \exp(i\mathbf{k} \cdot \mathbf{b}) + \exp(i\mathbf{k} \cdot \mathbf{c}) \} \\ - D(k) \{ \exp(-i\mathbf{k} \cdot \mathbf{a}/2) + \exp(-i\mathbf{k} \cdot \mathbf{b}/2) \\ + \exp(-i\mathbf{k} \cdot \mathbf{c}/2) \} , \quad (2.8a)$$

where

$$C(k) = \frac{Z_1 - \frac{2}{3} \exp(-k^2/8\alpha)}{1 + 2 \exp(-\alpha R^2/2)} , \quad (2.8b)$$

$$D(k) = \frac{\frac{4}{3} \exp(-k^2/8\alpha) \exp(-\alpha R^2/2)}{1 + 2 \exp(-\alpha R^2/2)} . \quad (2.8c)$$

In order to understand the role of bound electrons quantitatively, it is instructive to show $\rho_{\text{ext}}(k)$ for energetic cluster ions, i.e., a diproton (composed of two protons) and a triproton (composed of three protons with a triangular structure). We can easily obtain for a diproton

$$\rho_{\text{ext}}(\mathbf{k}) = 2Z_1 \cos(\mathbf{k} \cdot \mathbf{R}/2) , \quad (2.9a)$$

and for a triproton

$$\rho_{\text{ext}}(\mathbf{k}) = Z_1 \{ \exp(i\mathbf{k} \cdot \mathbf{a}) + \exp(i\mathbf{k} \cdot \mathbf{b}) \\ + \exp(i\mathbf{k} \cdot \mathbf{c}) \} . \quad (2.9b)$$

In Sec. III, the square of $\rho_{\text{ext}}(k)$ for a diproton ($2H^+$) and a triproton ($3H^+$), averaged over the angle of \mathbf{k} , are compared with those for H_2^+ and H_3^+ .

In this paper, we consider for a H_2^+ ion three types of correlations of the molecular axis with the direction of motion: (i) the molecular axis is fixed to be parallel to the direction of motion (referred to as PARA), (ii) the axis is fixed to be perpendicular to the direction of motion (referred to as PERP), and (iii) the axis is randomly oriented (referred to as SPHER) during the passage of a H_2^+ ion. Regarding the H_3^+ ion, the SPHER case only is considered and compared with the same case of the H_2^+ ion.

Next, let us briefly derive the stopping power formulas appropriate to the present case. The dynamic response of the medium is described by the dielectric function $\epsilon(\mathbf{k}, \omega)$. In the Fourier space, the induced potential $\phi_{\text{ind}}(\mathbf{k}, \omega)$ in the medium is given by

$$\phi_{\text{ind}}(\mathbf{k}, \omega) = \{1/\epsilon(\mathbf{k}, \omega) - 1\} (4\pi/k^2) \rho_{\text{ext}}(\mathbf{k}, \omega). \quad (2.10)$$

Then the stopping power, $S = -dE/dx$, is calculated as

$$S = \int d\mathbf{r} \rho_{\text{ext}}(\mathbf{r}, t) (-1/v) (\partial/\partial t) \phi_{\text{ind}}(\mathbf{r}, t). \quad (2.11)$$

Substituting (2.10) into (2.11) and using the Fourier transform (2.6a) of $\rho_{\text{ext}}(\mathbf{r}, t)$, one has within the linear response

$$S = -(1/2\pi^2 v) \int d\mathbf{k} (1/k^2) \int_{-\infty}^{\infty} d\omega \omega \text{Im}\{1/\epsilon(\mathbf{k}, \omega)\} [\rho_{\text{ext}}(\mathbf{k})]^2 \delta(\omega - \mathbf{k} \cdot \mathbf{v}). \quad (2.12)$$

In the wave-packet treatment, the electronic stopping power S of a material can be estimated as $S = S_{\text{cond}} + \sum_i S_i$, where S_{cond} and S_i denote, respectively, the stopping power of the conduction electrons and that of the bound electrons in the i th inner shell. These quantities, S_{cond} and S_i , are written explicitly as follows:

$$S_{\text{cond}} = (2/\pi v^2) (2k_F v_F)^2 \int_0^{\infty} dz z \int_0^{v/v_F} du u \text{Im}\{-1/\epsilon_L(z, u)\} f_{\text{ext}}^c(z, u, \alpha, R), \quad (2.13a)$$

$$S_i = (2/\pi v^2) (2q_i v_i)^2 \int_0^{\infty} dz z \int_0^{v/v_i} du u \text{Im}\{-1/\epsilon(z, u)\} f_{\text{ext}}^i(z, u, \alpha, R). \quad (2.13b)$$

In Eq. (2.13a), $\epsilon_L(z, u)$ denotes the Lindhard dielectric function [29] expressed in the reduced variables $z = k/(2k_F)$ and $u = \omega/(kv_F)$, with the Fermi wave number k_F and the Fermi velocity v_F . On the other hand, the complex dielectric function $\epsilon(z, u)$ in Eq. (2.13b) describing the dynamical polarization of the bound electrons was analytically obtained [30] and is characterized by the wave-number parameter $q_i = (N_i)^{1/3} Q_i$ (see Table I). Here, N_i is the number of electrons in the i th electronic shell per atom, and Q_i is determined by the one-electron Hartree-Fock momentum distribution at the origin $k = 0$. Using q_i , we define v_i , z , and u in Eq. (2.13b) as $v_i = \hbar q_i/m$, $z = k/(2q_i)$, and $u = \omega/(v_i k)$. The functions $f_{\text{ext}}^c(z, u, \alpha, R)$ and $f_{\text{ext}}^i(z, u, \alpha, R)$ indicate the square of the external charge $[\rho_{\text{ext}}(\mathbf{k})]^2$ expressed in the reduced variables z and u , which should be of the form relevant to the above three alignments. To survey the electron excitation in solid targets, we first restrict ourselves to Eq. (2.13a). In the SPHER case, by averaging $[\rho_{\text{ext}}(\mathbf{k})]^2$ over the angle between \mathbf{k} and \mathbf{R} , one can obtain

$$f_{\text{ext}}^c(z, u, \alpha, R) = [A(2k_F z)]^2 (\frac{1}{2}) \{1 + \sin(2k_F z R)/(2k_F z R)\} + [B(2k_F z)]^2 - 2A(2k_F z)B(2k_F z) \sin(k_F z R)/(k_F z R). \quad (2.14a)$$

Next, for the PERP case, one has

$$f_{\text{ext}}^c(z, u, \alpha, R) = (\frac{1}{2}) [A(2k_F z)]^2 [1 + J_0(2k_F z R \{1 - (v_F u/v)^2\}^{1/2})] + [B(2k_F z)]^2 - 2A(2k_F z)B(2k_F z) J_0(k_F z R \{1 - (v_F u/v)^2\}^{1/2}). \quad (2.14b)$$

Here $J_0(x)$ is the zeroth-order Bessel function of the first kind. Finally, for the PARA case, one can get

$$f_{\text{ext}}^c(z, u, \alpha, R) = [A(2k_F z) \cos(R\omega/2v) - B(2k_F z)]^2 = [A(2k_F z) \cos(Rk_F v_F z u/v) - B(2k_F z)]^2. \quad (2.14c)$$

In addition, for the SPHER case of the H_3^+ incidence, one can obtain

$$f_{\text{ext}}^c(z, u, \alpha, R) = [C(2k_F z)]^2 3 \{1 + 2g(2k_F z R)\} + [D(2k_F z)]^2 3 \{1 + 2g(k_F z R)\} - 6C(2k_F z)D(2k_F z) \{g(\sqrt{3}k_F z R) + 2g(k_F z R)\}, \quad (2.15)$$

where $g(x) = \sin(x)/x$.

Regarding $f_{\text{ext}}^i(z, u, \alpha, R)$ in Eq. (2.13b), replacement of variables k_F and v_F in $f_{\text{ext}}^c(z, u, \alpha, R)$ [Eqs. (2.14)–(2.15)] by q_i and v_i leads to the corresponding expressions for the H_2^+ orientations (SPHER, PERP, and PARA) and the H_3^+ orientation (SPHER). Therefore, we do not write them again. It is noted that in the cases of both the H_2^+ and H_3^+ ions, the functions $f_{\text{ext}}^c(z, u, \alpha, R)$ and $f_{\text{ext}}^i(z, u, \alpha, R)$ at $z = 0$ (or $k = 0$) equal unity, i.e., the square net charge of the projectiles, regardless of molecular orientations and the spatial size of

bound electrons.

As a final presentation in this section, we define the effective stopping-power charge Z_{eff} by

$$Z_{\text{eff}} = \{S/S_p\}^{1/2}. \quad (2.16)$$

This means the square root of the stopping power for an ion relative to that for a proton with equivalent velocity. A little attention should be paid to this. In general, this quantity is contributed by two effects, i.e., the charge-changing effect during the passage of the ion and the spatial-size effect of bound electrons attached to the ion.

TABLE I. The values of parameters, Q_i , N_i , r_s , and N_f , necessary for calculating Eqs. (2.13a) and (2.13b) for Al, C, and Kr targets. (A, B) means either $Q_i = A$ and $N_i = B$ for an inner shell i , or $r_s = A$ and $N_f = B$ for conduction electrons per atom.

Shell (i)	Al	C	Kr
1s	(7.276,2)	(3.268,2)	(21.00,2)
2s	(1.713,2)		(5.888,2)
2p	(1.625,6)		(6.281,6)
3s			(2.199,2)
3p			(2.078,6)
3d			(1.898,10)
4s			(0.7115,2)
4p			(0.5679,6)
Free	(2.070,3)	(1.526,4)	

Here we treat, however, the ions whose charge state is frozen, where the spatial distribution of bound electrons does not change during the penetration. Therefore, the charge-changing effect cannot be incorporated, and in this sense only the screening effect of bound electrons is purely reflected in Z_{eff} .

III. RESULTS AND DISCUSSION

First we describe general features of elementary excitations in the electron gas induced by energetic ions, since these excitations are dominant energy-loss mechanisms in solids up to several hundred keV/amu. As we know, there are two types of elementary excitations, i.e., the individual and the collective (plasmon) excitations [29]. The collective excitation mode can be restricted in the region of small momentum transfer, i.e., $0 \leq \hbar k \leq \hbar k_c$. Here, the cutoff wavelength k_c is at most the order of 1 a.u. Therefore, $\rho_{\text{ext}}(k)$ at relatively small k values, or, roughly speaking $\rho_{\text{ext}}(0)$, plays a dominant role. The threshold ion velocity V_{th} is characterized by $V_{\text{th}} = \omega_p / k_c$ if the dispersion of a plasmon is ignored. On the other hand, the individual excitation takes place over a wider range of momentum transfer and energy transfer. Then, in the individual excitation, the values of $\rho_{\text{ext}}(k)$ over the whole allowed section of k , depending on the velocity, affect the stopping power. This is a contrast to the case of the collective excitation.

In order to show how largely the screening effect by bound electrons works, the spherically averaged square external charge $\langle \rho_{\text{ext}}(k)^2 \rangle$ is plotted against k in Fig. 1(a) for a H_2^+ ion and a diproton ($2H^+$), and in Fig. 1(b) for a H_3^+ ion and a triproton ($3H^+$). At $k=0$, $\langle \rho_{\text{ext}}(k)^2 \rangle$ indicates the square net-charge values 1, 4, 1, and 9, respectively, in units of e^2 for H_2^+ , $2H^+$, H_3^+ , and $3H^+$, regardless of the internuclear distance R . Thus the bound electron diminishes the electron-excitation probability in a small momentum-transfer region. In this sense, the probability of the plasmon excitation induced by H_2^+ and H_3^+ ions is expected to be highly suppressed in comparison with $2H^+$ and $3H^+$ ions and to be almost the same as by a proton with the same velocity. On the contrary, in the small k regime, if k exceeds 4 a.u., there is no appreciable difference in $\langle \rho_{\text{ext}}(k)^2 \rangle$ between a H_2^+ (H_3^+) and a $2H^+$ ($3H^+$) ion. Then, in this k region, the bound electron does not play any role. This aspect will

be seen in the stopping cross sections calculated for aluminum and carbon as typical examples of solids, and for krypton as an example of gases.

Figure 2(a) shows the stopping power of a plasmon excited in a solid of $r_s = 2.07$ (Al) for penetrating H^+ , H_2^+ (SPHER, PARA, and PERP), and H_3^+ (SPHER) ions. As expected from Fig. 1, the net charges of these ions are the same value so that the resultant plasmon excitation contribution naturally yields almost the same result, regardless of the above ion species. On the contrary, the stopping cross section of the individual electron excitation shown in Fig. 2(b) displays a variety of curves, depending on the orientation of the molecular axis with respect to the direction of motion. In the low specific-energy region, the stopping curves for the SPHER H_3^+ , the PERP H_2^+ , the SPHER H_2^+, H^+ , and the PARA H_2^+ appear in order of magnitude. Above 400 keV/amu, three curves for the H_2^+ ions tends to converge and the orientation effect will disappear. Figures 2(a) and 2(b) imply that the individual excitation dominantly contributes to the orientation effect on the electronic stopping power for the H_2^+ incidence rather than the collective excitation. Physically speaking, a plasmon cannot be affected by the separation of constituent nuclei but can be affected by only the net charge since its wavelength λ_p is much larger than the internuclear distance R . For comparison, we calculated the above two contributions for a $2H^+$ ion, shown in Figs. 3(a) and 3(b). A $2H^+$ cluster has twice the net charge as a proton; as a result, the stopping power due to collective excitation amounts to four times the net charge, regardless of the $2H^+$ orientations. Except for

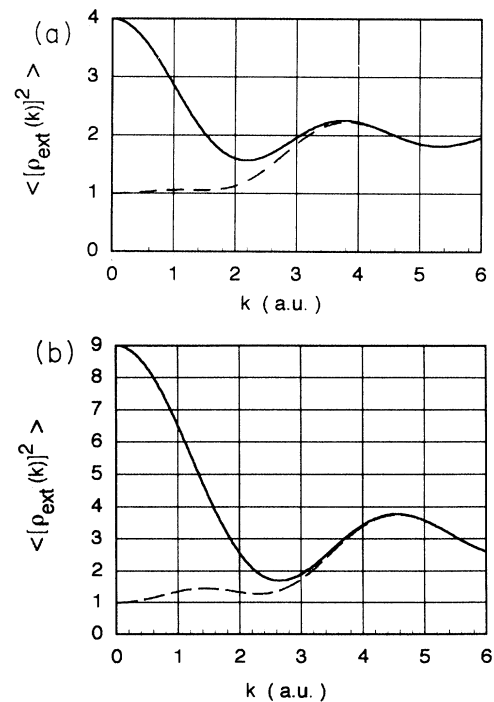


FIG. 1. (a) The square of the external charge, $\langle \rho_{\text{ext}}(k)^2 \rangle$, which is spherically averaged over molecular axes for H_2^+ (---) and a diproton ($2H^+$) (—). (b) Same as in (a) for H_3^+ (---) and a triproton ($3H^+$) (—).

the magnitude of the plasmon stopping, its orientation dependence for a 2H^+ cluster is very weak and similar to that for a H_2^+ ion. Figure 3(b) shows the stopping power of the individual excitation contribution for a moving 2H^+ ion. Compared with the case of H_2^+ shown in Fig. 2(b), the orientation dependence is qualitatively the same, except for the fact that the stopping value for 2H^+ is greater than for a H_2^+ ion with the same velocity. As a summary of this part, the orientation effect on the electronic stopping power actually works in the individual excitation process.

To clarify how the orientation effect works, we plot in Figs. 4(a)–4(d) the integrand, $zu f_{\text{ext}}^c(z, u, \alpha, R) \text{Im}\{-1/\varepsilon_L(z, u)\}$, in Eq. (2.13a) for the H_2^+ incidence at $v=4v_0$ on the electron gas of the density n_0 or $r_s=1.526$ [$1/n_0=(4\pi/3)(r_s a_0)^3$], which is deduced from the plasmon energy $\hbar\omega_p=25$ eV of carbon. For the incidence of a proton, the maximum peak is located at the same position ($z=0.4, u=1.2$) in the z - u plane when the incident velocity is greater than $1.6v_0$. This peak accompanies a broad tail within the region of $|z-u|<1$. As one easily sees from the borders of integration over u , each profile is obtained by truncating the universal profile at $u=v/v_F$. As well as the proton incidence, a profile of the SPHER H_2^+ incidence at finite velocity v is a truncation of the universal one, although there are humps originating from the oscillatory structure of $f_{\text{ext}}^c(z, u, \alpha, R)$. In the above two cases, we find no frequency dependence incorporating in $f_{\text{ext}}^c(z, u, \alpha, R)$. On the contrary, in the PARA and PERP cases, the frequency depen-

dence is expected to appear in the profile of $zu f_{\text{ext}}^c(z, u, \alpha, R) \text{Im}\{-1/\varepsilon_L(z, u)\}$. In the PERP case, except for the velocity-dependent undulations, the qualitative feature is similar to the SPHER one. The most remarkable aspect is the fact that the profile in the PARA case is constructed from several mountains separated by valleys. The valley lines are described by hyperbolic curves

$$zu = v / (Rk_F v_F) [(2n+1)\pi/2 + \arccos\{B(2k_F z) / A(2k_F z)\}]$$

$$(n=0, 1, 2, \dots)$$

As a common feature, the highest peak appears at the same position in the z - u plane. The above features are qualitatively valid for the profiles of the corresponding quantity $zuf_{\text{ext}}^i(z, u, \alpha, R) \text{Im}\{-1/\varepsilon(z, u)\}$ in Eq. (2.13b). These aspects reflect the molecular effects on the electronic excitation and lead us to a reasonable understanding of the orientation-dependent energy losses of H_2^+ , H_3^+ , 2H^+ , and 3H^+ ions displayed below.

A. H_2^+ and H_3^+ ions

The wave-packet procedure was found to present the Z_2 oscillation and the energy dependence of the electronic stopping cross section of materials, which are in relatively good agreement with the experimental and the empirical data available [30,31]. In this section, we show the calculated results for the molecular-ion incidence and compare them with the existing data. Here we concentrate on the solid Al and C targets, and a Kr gas target,

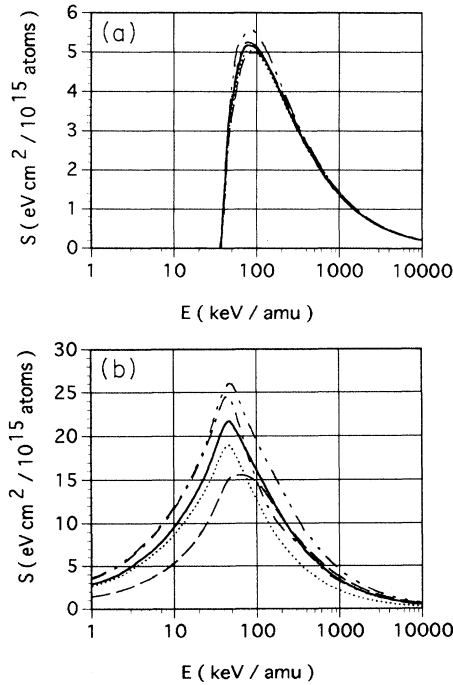


FIG. 2. (a) Stopping cross section of the plasmon excitation in an electron gas of $r_s=2.07$: H^+ ($\cdot\cdot\cdot$), H_2^+ (SPHER) (—), H_2^+ (PARA) (---), H_2^+ (PERP) (- - -), and H_3^+ (SPHER) (- - -). (b) Stopping cross section of the individual excitation in an electron gas of $r_s=2.07$. Legends are the same as in (a).

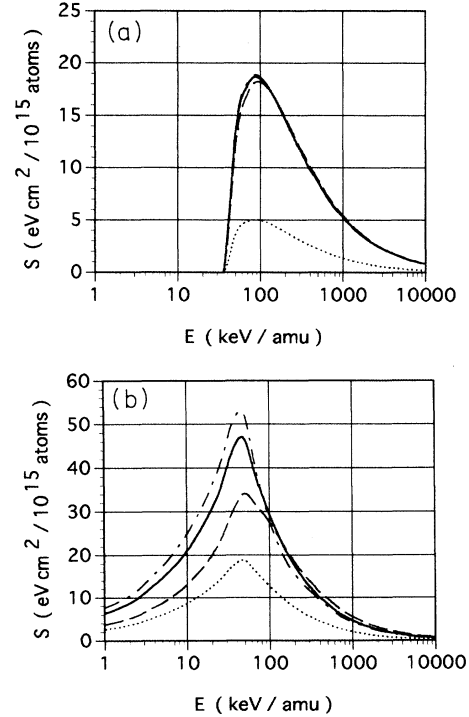


FIG. 3. (a) Stopping cross section of the plasmon excitation in an electron gas of $r_s=2.07$: H^+ ($\cdot\cdot\cdot$), 2H^+ (SPHER) (—), 2H^+ (PARA) (---), and 2H^+ (PERP) (- - -). (b) Stopping cross section of the individual excitation in an electron gas of $r_s=2.07$. Legends are the same as in (a).

for which calculation was carried out over the specific-energy range of $1 \text{ keV/amu} \leq E \leq 10 \text{ MeV/amu}$. Figure 5 shows the electronic stopping cross section S of Al for the H_2^+ ions in three orientations and the H_3^+ ion mentioned. For reference, the stopping cross section S_p of Al for a proton is drawn together. Comparison of the calculated S_p with the experimental S_p data was already made in other articles [30–32], which shows good agreement over the energy range studied. The shellwise calculation for a solid Al target reveals that the excitation of conduction electrons is dominant up to $\sim 100 \text{ keV/amu}$, but

once the specific energy is beyond this value the total stopping power would be no longer in agreement with the data without including the inner-shell ($1s, 2s, 2p$) contributions [31]. Here two $3s$ electrons and one $3p$ electron per aluminum atom are assumed to take part in the conduction electrons. In Fig. 5, S and S_p at low energies are proportional to $E^{1/2}$. Small shoulders around 600 keV/amu come from the $2s$ and $2p$ contributions. From this figure, one can see that S does strongly depend on the orientation of the molecular axis. The PERP orientation yields the greatest value in the energy region of $E < 80$

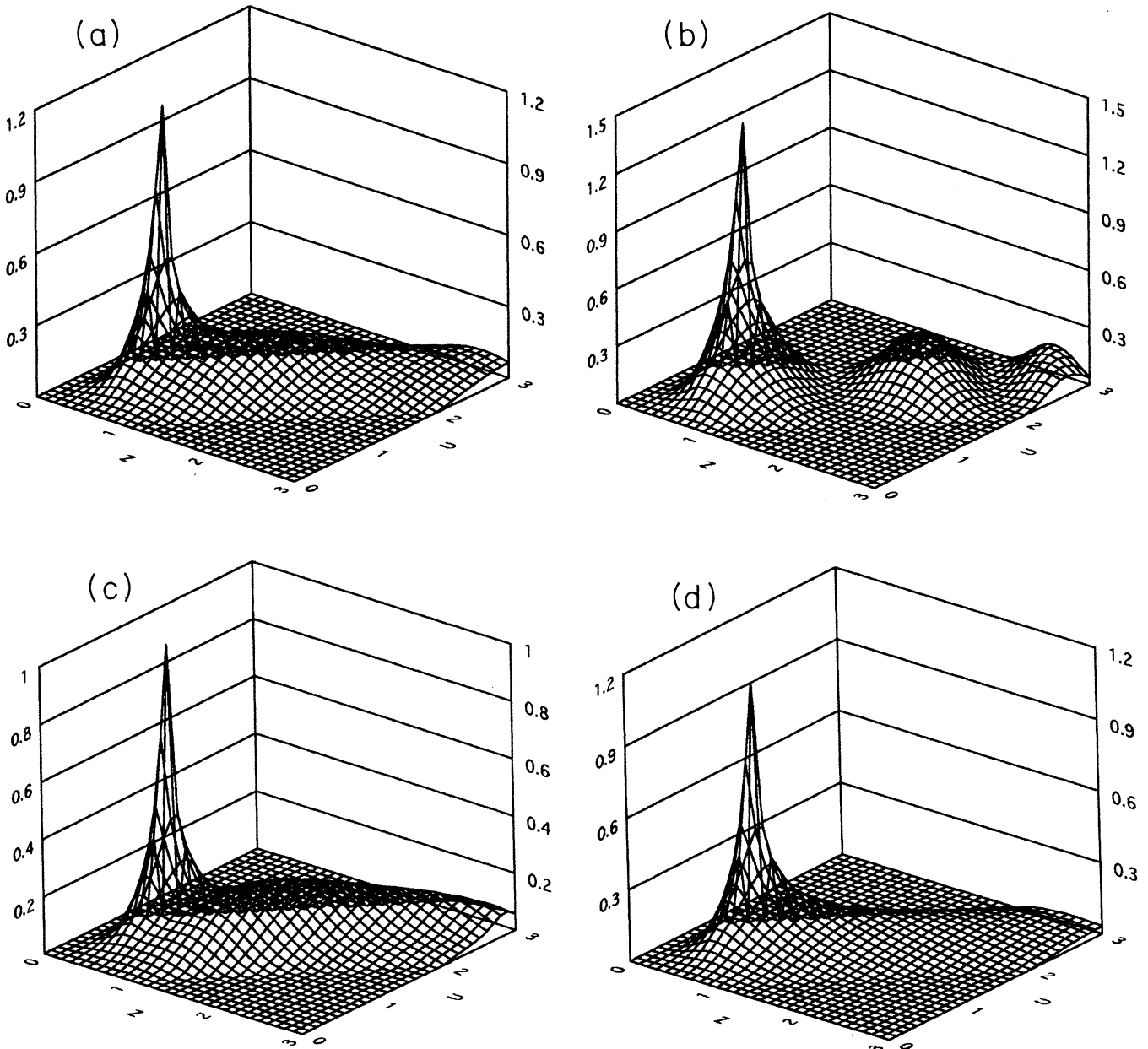


FIG. 4. Two-dimensional plots of the function, $z u f_{\text{ext}}^c(z, u, \alpha, R) \text{Im}\{-1/\epsilon_L(z, u)\}$, in Eq. (2.10a) in the ranges of $0 \leq z \leq 3$ and $0 \leq u \leq 3$ for the incidence of (a) the H_2^+ SPHER; (b) the H_2^+ PARA; (c) the H_2^+ PERP, and (d) the H^+ at $v=4v_0$ on the electron gas with $r_s = 1.526$.

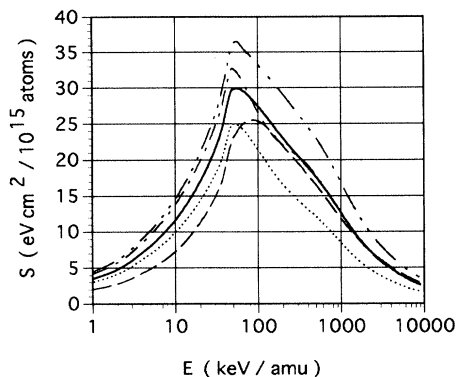


FIG. 5. Calculated stopping cross section S of Al for the H_2^+ incidence [SPHER (—), PARA (---), and PERP (- - -)] and for the SPHER H_3^+ incidence (— - -). For references, the stopping cross section S_p for the H^+ incidence (· · ·) is drawn together.

keV/amu. However, as E is over 200 keV/amu, the difference in three orientations becomes smaller with increasing E . The SPHER H_2^+ , the PERP H_2^+ , and the SPHER H_3^+ curves take a maximum at about $E=50$ keV/amu, as the proton curve does. On the other hand, the PARA H_2^+ curve becomes maximum at about $E=80$ keV/amu. At low energies, the SPHER H_3^+ curve is close to the PERP H_2^+ one. A remarkable aspect is that in the region of $E < 80$ keV/amu the stopping cross section S for the PARA H_2^+ is always less than that for a proton at the same velocity. This tendency is valid for another solid target(C) as well as a gaseous target(Kr), which implies that it is a rather general aspect regardless of target species. Figures 6 and 7 indicate the electronic stopping cross sections of carbon and krypton, respectively, for a H_2^+ ion, a H_3^+ ion, and a proton. The SPHER H_2^+ , and PERP H_2^+ , the SPHER H_3^+ , and the proton curves of carbon(krypton) take a maximum at about $E=80$ keV/amu (100 keV/amu), while the PARA H_2^+ curve of carbon(krypton) becomes maximum at about $E=130$ keV/amu (150 keV/amu). Except for the shift of peak values towards the higher energy side, the orientation dependence of the stopping curves of carbon

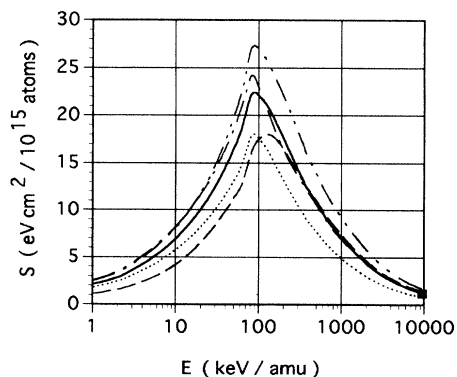


FIG. 6. Calculated stopping cross section S of C for the H_2^+ incidence. Legends are the same as in Fig. 5. The experimental data is obtained for 9.6 MeV/amu H_2^+ by Susuki *et al.* [33].

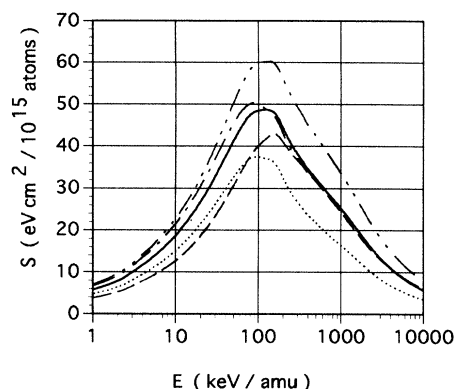


FIG. 7. Calculated stopping cross section S of Kr for the H_2^+ incidence. Legends are the same as in Fig. 5.

and krypton for a H_2^+ ion is qualitatively the same as those of aluminum. The solid square symbol in Fig. 6 is the data of the recent measurement done by Susuki *et al.* [33] using 9.6 MeV/amu H_2^+ ions. In this experiment, a H_2^+ ion is assumed to be in the spherical orientation, which agrees with the calculated one. As the kinetic energy increases, the orientation effect tends to disappear. From Figs. 5–7, one finds that the stopping cross section for a H_3^+ ion is greater than those for a H_2^+ ion especially at high energies, though the profile is similar and the net charge is the same. This enhancement is caused by the close collision (i.e., the individual excitation) contribution, while the distant collision (i.e., the collective excitation) contribution is almost the same [see Fig. 2(a)].

Figures 8–10 display the effective stopping-power charge Z_{eff} of a H_2^+ ion in collision with Al, C, and Kr targets, respectively. For comparison, the effective charge of a He^+ ion is also plotted as a function of the specific energy. Because we have interest in the limiting case of vanishing R for a H_2^+ ion, which reduces to a point charge (He^+). The orbital parameter α for He^+ is calculated to be 1.132 a.u. by applying a variational method to minimization of the energy as in Eqs. (2.2) and

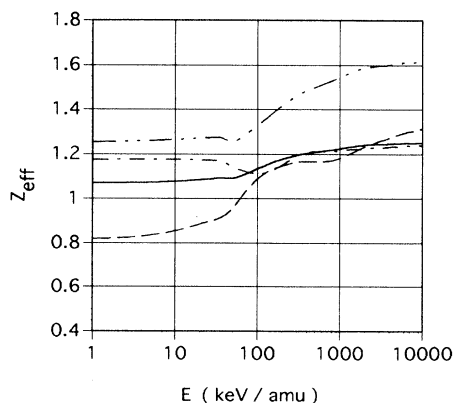


FIG. 8. Effective charge Z_{eff} of the H_2^+ incident on Al: SPHER (—), PARA (---), and PERP (- - -). For reference, Z_{eff} of the He^+ incidence on Al (— - -) is drawn together.

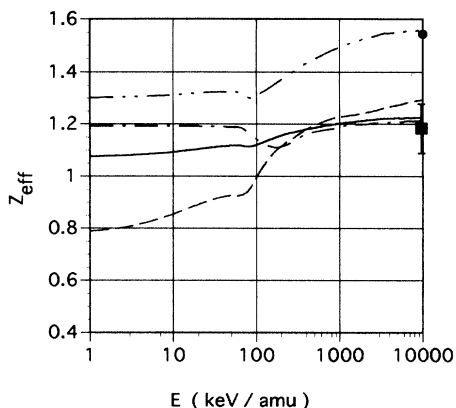


FIG. 9. Effective charge Z_{eff} of the H_2^+ incident on C. Legends are the same as in Fig. 8. The solid circle and the solid square are the experimental data obtained for the 10.7 MeV/amu He^+ by Ogawa *et al.* [23] and for the 9.6 MeV/amu H_2^+ by Susuki *et al.* [33].

(2.4). At a glance, three figures for H_2^+ indicate the strong orientation dependences at low energies (less than a few hundred keV/amu). In Fig. 9, the solid circle indicates the experimental data ($Z_{\text{eff}}=1.54$) obtained by Ogawa *et al.* for the 32 MeV/amu $^3He^+$ ion in the pre-equilibrium charge state [23]. The solid square is the data of Susuki *et al.* for the 9.6 MeV/amu H_2^+ ion in the frozen charge state [33]. From Figs. 8–10, the following characters can be found on Z_{eff} of H_2^+ ions.

(i) In the PARA and SPHER cases, Z_{eff} increases monotonically with increasing specific energy E , while in the PERP case the Z_{eff} tends to be almost constant (~ 1.2) over the energies studied except for a shallow dip around 100–200 keV/amu.

(ii) In the PARA case, Z_{eff} is less than unity up to ~ 100 keV/amu.

(iii) Z_{eff} of the PARA case varies considerably from 0.8 (for Al and C) ~ 0.9 (for Kr) to ~ 1.3 , while Z_{eff} of the SPHER changes slightly from ~ 1.1 to ~ 1.25 and in the PERP the variation of Z_{eff} amounts to ~ 0.1 .

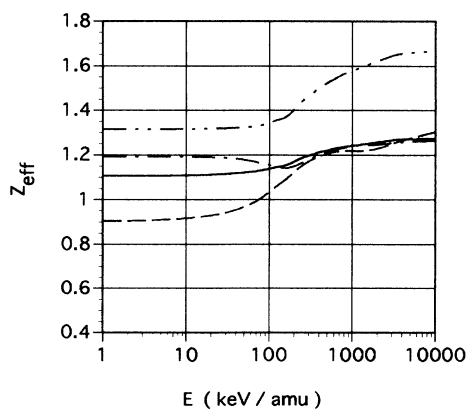


FIG. 10. Effective charge Z_{eff} of the H_2^+ incident on Kr. Legends are the same as in Fig. 8.

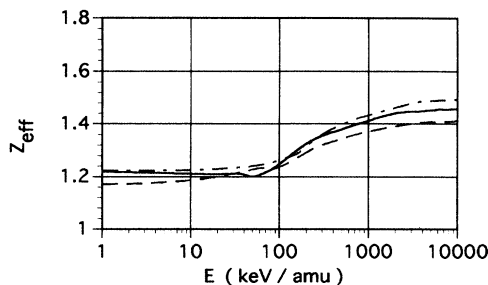


FIG. 11. Effective charge Z_{eff} of the H_3^+ (SPHER) incident on Al (—), on C (---), and on Kr (- - -).

(iv) At low energies, a strong orientation dependence in Z_{eff} is found, and as the kinetic energy exceeds several hundred keV/amu, the differences in the stopping power and the effective charge for oriented H_2^+ ions tends to vanish.

(v) Z_{eff} value of a H_2^+ ion is always less than that of a He^+ ion at identical velocities.

The second point (ii) reveals that the bound electron on a projectile and the orientation of the molecular axis cooperate with each other to diminish. Keep in mind that only one of them cannot derive this result. In the next section, we compare the Z_{eff} values of $2H^+$ and $3H^+$ ions with those of H_2^+ and H_3^+ ions, and clarify the difference in Z_{eff} .

To check to what extent the choice of R is sensitive, we calculated the stopping of Al for the vibrationally averaged internuclear distance $R = 1.29$ (Å) [8] of a H_2^+ ion. Compared with the case of the ground-state distance $R = 1.084$ (Å), Z_{eff} decreases by at most 0.05 only in the low- E region and any drastic variations cannot be found in the Z_{eff} curves for H_2^+ in three orientations in Al.

In addition to the H_2^+ incidence, Z_{eff} of the SPHER H_3^+ incident on Al, C, and Kr targets is shown in Fig. 11. In the range of $1 \text{ keV/amu} \leq E \leq 10^4 \text{ keV/amu}$, Z_{eff} changes from 1.2 to 1.46 for Al, from 1.17 to 1.41 for C, and from 1.22 to 1.49 for Kr. The following remarks should be added.

(vi) Z_{eff} of the SPHER H_3^+ depends weakly on target species.

(vii) The profile of Z_{eff} of the SPHER H_3^+ resembles that of the SPHER H_2^+ . In practice, the ratio R_z of Z_{eff} of the SPHER H_3^+ to that of the SPHER H_2^+ is almost constant at the kinetic energies ranging from 1 keV/amu to 10^4 keV/amu: $R_z = 1.09$ – 1.15 (C), 1.10 – 1.165 (Al), and 1.11 – 1.174 (Kr).

The variation of Z_{eff} of the SPHER H_3^+ ions is about 0.24–0.27 over the energy range of $1 \text{ keV/amu} \leq E \leq 10^4 \text{ keV/amu}$. Ordinarily, in such a wide energy range, the effective charge of a single ion tends to vary more. For example, Z_{eff} for He^+ in a frozen charge state changes from 1.26 to 1.62 in Al, and if the charge-changing process is included, from ~ 1.3 to 2 in solids and gaseous targets [34].

B. $2H^+$ and $3H^+$ ions

In order to make clear the differences between a diproton and a H_2^+ ion and between a triproton and a H_3^+ ion, we also calculate the stopping cross section for diproton ($2H^+$) clusters in the SPHER, PARA, and PERP orientations, and for a triproton ($3H^+$) cluster in the SPHER one. Here the internuclear distances of a $2H^+$ ion and a $3H^+$ ion are fixed to be 1.084 and 0.897 Å, respectively, so that the Coulomb explosion is not taken into account. Figures 12–14 show the stopping cross sections of Al, C, and Kr targets, respectively, for $2H^+$ clusters. As for Al and C targets, the stopping cross section increases steeply around 40 keV/amu and 60 keV/amu, where the plasmon excitation begins to contribute. As a common feature, below ~ 100 keV/amu the PERP curve is the largest among four curves, and the SPHER, the PARA, and the proton curves follow in order of magnitude. It is remarkable that, different from the H_2^+ case, the PARA curve is greater than the proton curve for each target. On the other hand, as is similar to the H_2^+ case, the orientation dependence of the stopping is not appreciated as far as the specific energy is beyond 200 keV/amu. Regarding the $3H^+$ case, the profiles of the stopping curve of these targets are qualitatively the same as those for the $2H^+$ SPHER case. One can confirm this point by comparing the Z_{eff} curves. Figures 15–17 display the effective charge of $2H^+$ and $3H^+$ in collisions with Al, C, and Kr targets. The following features can be derived from these figures.

(i) Z_{eff} curves for the PERP $2H^+$ and the SPHER $2H^+$ in three targets vary by 0.2, while Z_{eff} for the PARA $2H^+$ changes by 0.4 over the kinetic energy E of $1 \text{ keV/amu} \leq E \leq 10^4 \text{ keV/amu}$.

(ii) Different from the PARA H_2^+ case, Z_{eff} values for $2H^+$ ions are greater than unity ($=Z_{\text{eff}}$ of a proton).

(iii) Z_{eff} of the PARA case varies considerably from 0.8 (for Al and C) ~ 0.9 (for Kr) to ~ 1.3 , while Z_{eff} of the SPHER changes slightly from ~ 1.1 to ~ 1.25 and in the PERP the variation of Z_{eff} amounts to ~ 0.1 .

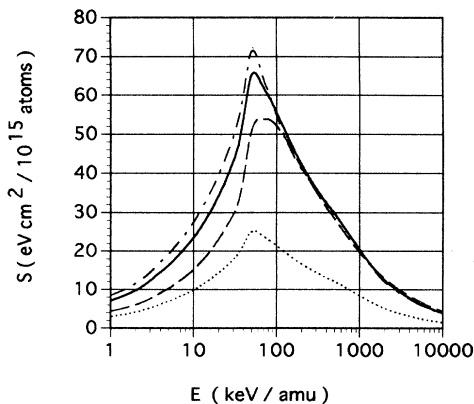


FIG. 12. Calculated stopping cross section S of Al for the $2H^+$ incidence: SPHER (—), PARA (---), and PERP (- - -). For reference, the stopping cross section S_p for the H^+ incidence ($\cdot \cdot \cdot$) is drawn together.

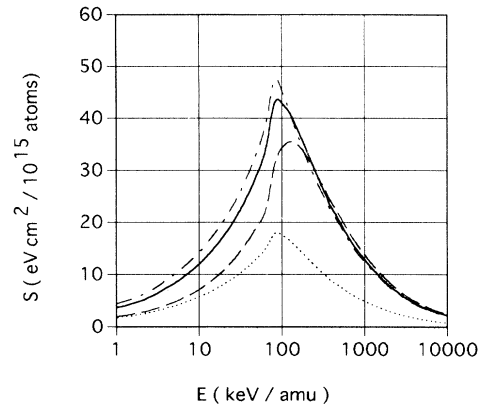


FIG. 13. Calculated stopping cross section S of C for the $2H^+$ incidence. Legends are the same as in Fig. 12.

(iv) At low energies, a strong orientation dependence in Z_{eff} of $2H^+$ is found: the PERP, the SPHER, and the PARA curves are in order of magnitude up to ~ 100 keV/amu. As the kinetic energy exceeds several hundred keV/amu, the orientation dependence of the Z_{eff} curves for the $2H^+$ ions tends to vanish.

(v) The profile of Z_{eff} for the SPHER $3H^+$ resembles that for the SPHER $2H^+$. In practice, the ratio R_z of Z_{eff} of the SPHER $3H^+$ to that of the SPHER $2H^+$ ion is almost constant at the kinetic energies ranging from 1 keV/amu to 10^4 keV/amu: $R_z = 1.37\text{--}1.41$ (C), $1.36\text{--}1.44$ (Al), and $1.34\text{--}1.40$ (Kr).

C. Screening effect

Contrasts between Sec. III A and Sec. III B reflect the role of the projectile electron. This is the effect of screening the nuclear charge effectively, which depends on the projectile velocity. To investigate it, we calculate the effective screening charge per bound electron ΔZ_{eff} defined by the following relations:

$$\Delta Z_{\text{eff}} = Z_{\text{eff}}(2H^+) - Z_{\text{eff}}(H_2^+) \quad (3.1a)$$

or

$$\Delta Z_{\text{eff}} = \left(\frac{1}{2}\right)[Z_{\text{eff}}(3H^+) - Z_{\text{eff}}(H_3^+)], \quad (3.1b)$$

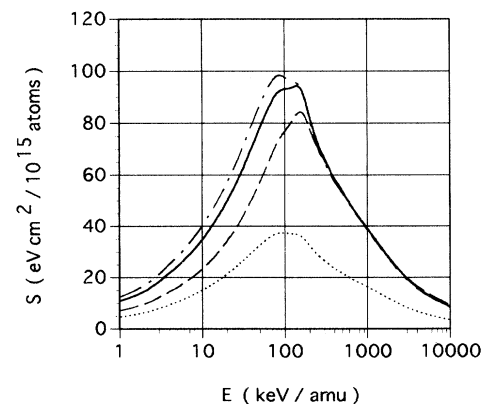


FIG. 14. Calculated stopping cross section S of Kr for the $2H^+$ incidence. Legends are the same as in Fig. 12.

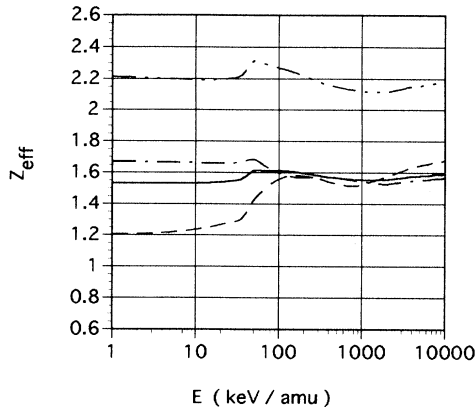


FIG. 15. Calculated effective charge Z_{eff} of the $2H^+$ incident on Al [SPHER (—), PARA (---), and PERP (- - -)] and for the $3H^+$ (SPHER) incidence (— · — · —).

where $Z_{\text{eff}}(2H^+)$ means the effective charge of $2H^+$, etc. Figure 18 indicates the energy dependence of ΔZ_{eff} for Al, C, and Kr targets. Except for details, the four profiles of ΔZ_{eff} in each target commonly have a similar structure. In Al and C targets, the humps located at 50–80 keV/amu are due to the enhanced plasmon contributions by a $2H^+$ ion and a $3H^+$ ion, rather than by a H_2^+ ion and a H_3^+ ion. Namely, in the plasmon excitation, the bound electron screens the projectile charge almost completely. This is straightforwardly understood by comparing Figs. 2(a) and 3(a). When the kinetic energy is over ~ 100 keV/amu, ΔZ_{eff} decreases with increasing energy. We can reasonably interpret this as follows: At high energies, a large momentum transfer becomes dominant and there, as indicated in Figs. 1(a) and 1(b), the square external charges of a $2H^+$ ion and a $3H^+$ ion are not so different from those of a H_2^+ ion and a H_3^+ ion, respectively, compared at lower energies. Roughly speaking, one bound electron on a H_2^+ or a H_3^+ ion diminishes the effective charge by 0.3–0.5.

Our calculation of Z_{eff} values of a $2H^+$ and a $3H^+$ cluster can be connected with the interference function G

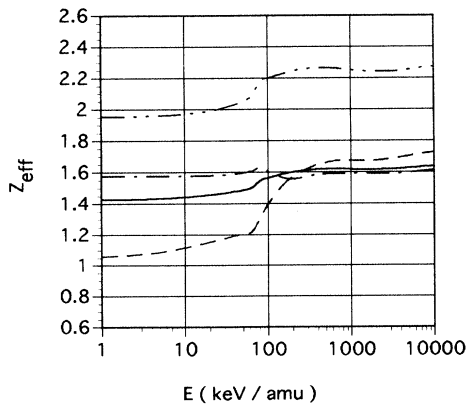


FIG. 16. Calculated effective charge Z_{eff} of the $2H^+$ incident on C. Legends are the same as in Fig. 15.

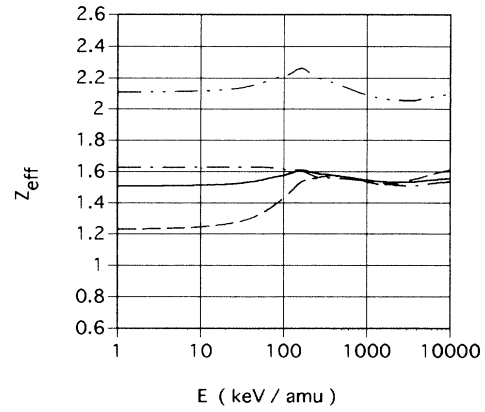


FIG. 17. Calculated effective charge Z_{eff} of the $2H^+$ incident on Kr. Legends are the same as in Fig. 15.

at the entrance. For a point-charge cluster composed of Z_1e and Z_2e , Brandt, Ratkowski, and Ritchie [8] write S in terms of

$$S = (e\omega_p/v)^2 \ln(2mv^2/\hbar\omega_p) [Z_1^2 + Z_2^2 + 2Z_1Z_2G]. \quad (3.2)$$

Hereby the effective charge becomes

$$Z_{\text{eff}} = [Z_1^2 + Z_2^2 + 2Z_1Z_2G]^{1/2}. \quad (3.3)$$

After averaging over the direction of \mathbf{R} , G reduces to a function of the variable $R\omega_p/v$. Taking into account the Coulomb explosion effect on the time-dependent internuclear distance $R(t)$, they roughly obtain $G = \frac{1}{2}$ for a swift $2H^+$ ion at the entrance ($t=0$). This means that Z_{eff} of

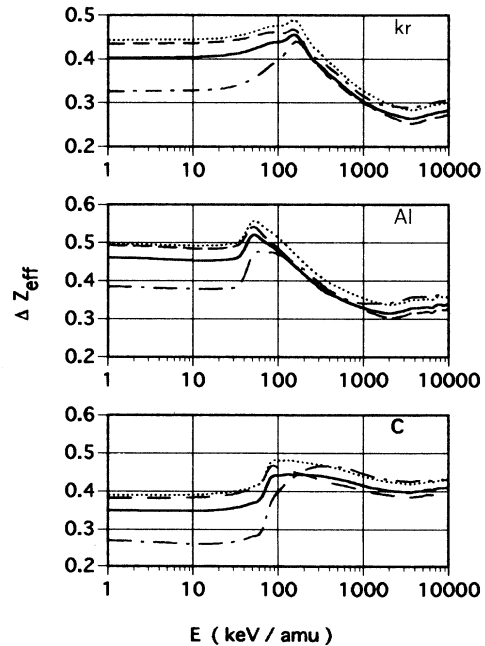


FIG. 18. Screening charge per bound electron for Kr, Al, and C targets, calculated from Eqs. (3.1a): [SPHER (—), PARA (---), PERP (- - -)] and from Eq. (3.1b) [SPHER (· · · ·)].

the SPHER 2H^+ is $(1+1+2\times\frac{1}{2})^{1/2}=1.732$. In the present case, Z_{eff} is 1.43–1.64 in C, 1.53–1.16 in Al, and 1.51–1.61 in Kr in the range of $1 \text{ keV/amu} \leq E \leq 10^4 \text{ keV/amu}$. Applying $G=\frac{1}{2}$ also to a 3H^+ ion, Z_{eff} of the SPHER 3H^+ amounts to $\{1+1+1+2\times(\frac{1}{2})\times 3\}^{1/2}=2.45$. We obtain that the corresponding Z_{eff} is 1.95–2.28 in C, 2.12–2.31 in Al, and 2.06–2.26 in Kr. Figures 15–17 show that the function G is energy, target, and orientation dependent. In addition, the values of G are found to be smaller than $\frac{1}{2}$, since Z_{eff} values of 2H^+ and 3H^+ are smaller than what are expected from $G=\frac{1}{2}$ in (3.3). Up to here, the Z_{eff} values of H_2^+ and H_3^+ ions in a frozen charge state are found to be smaller than both the correlated ($G=\frac{1}{2}$) value from the point-charge-cluster model [8] and the completely uncorrelated ($R=\infty$) value over the whole energy range studied. This is ascribed to the screening effect of the projectile's bound electron.

By the way, it was reported [20] that the energy loss per nucleon of a recombined H_2^+ ion at $v=0.7 v_0$ (12.5 keV/amu) and $v=v_0$ (25 keV/amu) incident on carbon is 0.8–0.9 times the corresponding proton stopping S_p . It means $Z_{\text{eff}}=1.26$ –1.34. This fact allows us to conclude that Z_{eff} of a recombined H_2^+ ion is larger than that of a H_2^+ ion in a frozen charge state (see Fig. 9). Though it is not a hydrogen-molecular ion, such a molecular-orientation effect has been also suggested. The reduction of the energy loss per nucleon of nitrogen-molecular ions incident on carbon was reported in the velocity regime of $v=1.2$ – $2.28v_0$ [21], where the reduction amounts to 15% at most and depends on the dwell time in the foil. On the basis of an electron-gas target with energy gap, Steuer and Ritchie [22] calculated the energy loss of a nitrogen-molecular ion in the parallel orientation. According to them, the theoretical reduction is 21–27%, which is larger than the 9–13% reduction in the experiment. Quantitative agreement has not been achieved yet. It is, however, demonstrated that the parallel orientation will be actually a promising candidate for explaining this reduction.

D. Summary

This paper presented the orientation effect on the inelastic energy loss of H_2^+ and H_3^+ ions *with bound electron(s) in a frozen charge state* penetrating carbon and aluminum foils and Kr gas. At low energies less than $\sim 100 \text{ keV/amu}$, the stopping power and the effective charge of H_2^+ strongly depend on the alignments of the molecular axis. These quantities are, even in any alignments, smaller than those of He^+ ions, which is regarded

as a H_2^+ ion with vanishing R . A special emphasis should be put on the fact that the stopping power (and the effective charge) for the parallel oriented H_2^+ with kinetic energy up to several 10 keV/amu amounts to 0.6–0.8 times as much as the proton stopping. This finding is common to three targets investigated in this paper. Here one pays attention to the magnitude of the stopping. According to the previous analysis based on the point-charge-cluster model, it was pointed out that due to the interference effect the stopping power *per proton* of carbon for H_2^+ in the parallel orientation is reduced at minimum to be 0.5 times as much as that for the proton at the same velocity [20] (namely, the stopping power for H_2^+ is equal to the proton stopping). So the stopping power for the H_2^+ in our case is much more suppressed. The role of bound electrons was very important especially for low-velocity hydrogen molecules and even at high velocities they can diminish the effective charge by 0.3–0.4 per electron.

Finally, we make a comment on the existence of binding states. The effect of screening the external charge by conduction electrons is important for low-velocity ions insofar as H_2^+ and H_3^+ ions can bind electron(s) in a solid. Apart from the proton incidence [35–37], no comprehensive works have been done on the existence of such a molecular-orbital bound state in a solid, to the author's knowledge. However, at least in the several hundred keV/amu to MeV/amu region, the original transmission of H_2^+ and H_3^+ ions has been observed through superthin foils [17,18], where the effect of the bound electrons is not vanishing even if the static screening effect becomes vanishing. Recent experiments [33] prove that the calculated results agree with the data. We would like to expect that by combining the measurement of charge-state fractions, the research on the stopping of molecular and cluster ions presents information on the alignment effects and the effective screening charge.

Note added in proof. Recently, Y. Susuki *et al.* (unpublished) measured the energy loss of the 9.6-MeV/amu H_3^+ ion incident on carbon, where the effective charge Z_{eff} derived from the stopping power data is $Z_{\text{eff}}=1.45\pm 0.09$. These data are in good agreement with our calculated value shown in Fig. 11.

ACKNOWLEDGMENTS

The author would sincerely like to thank Dr. Y. Susuki and co-workers for the courtesy of sending their manuscript prior to publication. Also, he appreciates a grant from Electric Technology Research Foundation of Chugoku.

- [1] M. J. Gaillard, J. C. Poizat, A. Ratkowski, J. Remillieux, and M. Auzas, *Phys. Rev. A* **16**, 2323 (1977).
- [2] M. J. Gaillard, J. C. Poizat, and J. Remillieux, *Phys. Rev. Lett.* **41**, 159 (1978).
- [3] N. Cue, M. J. Gaillard, J. C. Poizat, J. Remillieux, and J. L. Subtil, *Phys. Rev. Lett.* **42**, 959 (1979).
- [4] G. Astner, S. Mannervik, and E. Veje, *Nucl. Instrum. Methods Phys. Res.* **194**, 319 (1982).

- [5] R. Latz, G. Astner, H. J. Frischkorn, P. Koschar, J. Pfenning, J. Schader, and K. O. Groeneveld, *Nucl. Instrum. Methods Phys. Res.* **194**, 315 (1982).
- [6] H. Kobayashi and N. Oda, *Phys. Rev. A* **30**, 1294 (1984).
- [7] Y. Yamazaki and N. Oda, *Nucl. Instrum. Methods Phys. Res.* **194**, 323 (1982).
- [8] W. Brandt, A. Ratkowski, and R. H. Ritchie, *Phys. Rev. Lett.* **33**, 1325 (1974).

- [9] Z. Vager and D. S. Gemmell, Phys. Rev. Lett. **37**, 1352 (1976).
- [10] E. P. Kanter, P. J. Cooney, D. S. Gemmell, K.-O. Groeneveld, W. J. Pietsch, A. J. Ratkowski, Z. Vager, and B. J. Zabransky, Phys. Rev. A **20**, 834 (1979).
- [11] D. S. Gemmell, Nucl. Instrum. Methods Phys. Res. **194**, 255 (1982).
- [12] D. S. Gemmell, Chem. Phys. **80**, 301 (1980).
- [13] D. S. Gemmell, J. Remillieux, J.-C. Poizat, M. J. Gaillard, R. E. Holland, and Z. Vager, Phys. Rev. Lett. **34**, 1420 (1975).
- [14] N. R. Arista, Phys. Rev. B **18**, 1 (1978).
- [15] N. R. Arista and A. Gras-Marti, J. Phys. Condens. Matter **3**, 7931 (1991).
- [16] G. Basbas and R. H. Ritchie, Phys. Rev. A **25**, 1943 (1982).
- [17] N. Cue, N. V. de Castro-Faria, M. J. Gaillard, J. C. Poizat, J. Remillieux, D. S. Gemmell, and I. Plessier, Phys. Rev. Lett. **45**, 613 (1980).
- [18] N. Cue, N. V. de Castro-Faria, M. J. Gaillard, J. C. Poizat, and J. Remillieux, Phys. Lett. **72A**, 104 (1979).
- [19] J. C. Eckardt, G. Lantschner, N. R. Arista, and R. A. Baragiola, J. Phys. C **11**, L851 (1978).
- [20] R. Levi-Setti, K. Lam, and T. R. Fox, Nucl. Instrum. Methods Phys. Res. **194**, 281 (1982).
- [21] M. F. Steuer, D. S. Gemmell, E. P. Kanter, E. A. Johnson, and B. J. Zabransky, Nucl. Instrum. Methods Phys. Res. **194**, 277 (1982).
- [22] M. F. Steuer and R. H. Ritchie, Nucl. Instrum. Methods Phys. Res. Sect. B **33**, 170 (1988).
- [23] H. Ogawa, I. Katayama, H. Ikegami, Y. Haruyama, A. Aoki, M. Tosaki, F. Fukuzawa, K. Yoshida, I. Sugai, and T. Kaneko, Phys. Rev. B **43**, 11 370 (1991).
- [24] H. Ogawa, I. Katayama, I. Sugai, Y. Haruyama, M. Tosaki, A. Aoki, K. Yoshida, and H. Ikegami, Phys. Lett. A **167**, 487 (1992).
- [25] H. Ogawa, I. Katayama, I. Sugai, Y. Haruyama, M. Saito, K. Yoshida, M. Tosaki, and H. Ikegami, Nucl. Instrum. Methods Phys. Res. Sect. B **82**, 80 (1993).
- [26] Toshiaki Kaneko, Phys. Rev. A **43**, 4780 (1991); **49**, 2681 (1994).
- [27] T. Kaneko and H. Tsuchida, J. Phys. B **27**, 97 (1994).
- [28] G. D. Carney and R. N. Porter, J. Chem. Phys. **65**, 3547 (1976).
- [29] J. Lindhard and A. Winther, K. Dan. Vidensk. Selsk. Mat. Fys. Medd. **34** (4), 1 (1964).
- [30] Toshiaki Kaneko, Phys. Rev. A **40**, 2188 (1989); Phys. Status Solidi B **156**, 49 (1989).
- [31] Toshiaki Kaneko, At. Data Nucl. Data Tables **53**, 271 (1993).
- [32] H. Paul, M. J. Berger, and H. Bichsel, in *Atomic and Molecular Data Needed in Radiotherapy* (IAEA-TECDOC, Vienna, 1994), Chap. 7.
- [33] Y. Susuki, M. Fritz, K. Kimura, M. Mannami, N. Sakamoto, H. Ogawa, I. Katayama, T. Noro, and H. Ikegami, Phys. Rev. A **50**, 3533 (1994).
- [34] J. F. Ziegler, *He: The Stopping and Ranges of Ions in Matter* (Pergamon, New York, 1977).
- [35] F. J. Rogers, H. C. Graboske, Jr., and D. J. Harwood, Phys. Rev. A **1**, 1577 (1970).
- [36] M. C. Cross, Phys. Rev. B **15**, 602 (1977).
- [37] C. O. Almbladh, U. von Barth, Z. D. Popovic, and M. J. Scott, Phys. Rev. B **14**, 2250 (1976).